Physica Scripta. Vol. 35, 541–546, 1987.

# Electronic Resonances in Rare-Gas Adsorbates Observed by Spin-Resolved Electron Spectroscopy*

G. Schönhense, B. Kessler, N. Müller, B. Schmiedeskamp and U. Heinzmann

Universität Bielefeld, Fakultät für Physik, D-4800 Bielefeld, F.R.G.; Fritz-Haber-Institut der MPG, Faradayweg 4–6, D-1000 Berlin 33, F.R.G.

*Received August 8, 1986; accepted October 28, 1986*

**Abstract**

Recent experimental results of spin-polarized electron emission following photoexcitation of the valence orbitals of adsorbed rare-gas atoms are presented. As light source we employed the circularly polarized synchrotron radiation from the storage ring BESSY (Berlin). As detection technique served angle- and spin-resolved electron spectroscopy. The resolution of the experimental method is demonstrated by the example of photoemission from Ar on Pt(111), where a doublet feature with a splitting of only 90 meV could be resolved, which is hardly discernible in intensity spectroscopy. Below the threshold for direct photoemission narrow electronic resonances have been observed, resulting from discrete $np \rightarrow n's$ excitations in the adsorbate. For the system Xe on Ir(111) the dependence of the resonance features on the coverage from the sub-monolayer regime up to the 3D-crystal is discussed.

## 1. Introduction and experimental

Energy-, angle-, and spin-resolved photoelectron emission from solids and adsorbates has proven to be a valuable tool in the investigation of the electronic structure (for a recent review, see Ref. [1]). One basic potential of the new method is that it allows to probe the symmetries of electronic states, especially for high-$Z$ systems. For such elements the conventional technique of applying polarization selection rules for plane-polarized radiation fails because of strong mixing of orbital symmetries as a consequence of spin–orbit interaction. We have demonstrated the advantages of spin-resolved measurements for the determination of band symmetries by the examples of the Pt(111) crystal and adsorbed Xe and Kr atoms. For platinum, a symmetry-resolved bandmapping of the $\Lambda$-direction was performed [2] and for the adsorbed rare-gas atoms an unambiguous quantum-number labelling of the Xe $5p$ and Kr $4p$ hole states was given [3].

A very surprising experimental result was the discovery of sharp, photon-induced resonances in Kr and Xe adsorbates on Pt(111) and graphite(0001) [4]. Measurements of the electron-spin polarization (ESP) of the resonantly emitted electrons allowed to identify the resonances as discrete $np \rightarrow (n+1)s$ excitations, exhibiting an additional line splitting due to the anisotropic bonding interactions on the surface. In the present article we present new experimental data obtained for argon monolayers on the platinum(111) face and for xenon monolayers on the basal plane of natural single crystal graphite [5]. Furthermore, we demonstrate the sensitivity of the electronic resonances on the coverage by the example of xenon on the iridium(111) face from the sub-monolayer regime up to the three-dimensional xenon crystal.

The method of photoelectron spin-polarization spectroscopy and its experimental equipment has been recently described in some detail [6]. The method is based upon spin orientation by optical pumping with circularly polarized ($\sigma$) light and photoelectron spin detection by a conventional high-energy Mott detector (operated at a scattering energy of 100 keV) preceded by a special angle-resolving photoelectron spectrometer. The experiment is set up at the storage ring BESSY (Berlin), utilizing the circularly polarized off-plane synchrotron radiation delivered by the 6.5 m normal-incidence monochromator [7]. Target preparation is made in a separate preparation chamber equipped with an ion gun, a scanning Auger system and LEED optics. The substrate crystal is mounted on a liquid-helium cooled target manipulator; the crystal temperature can be varied between 40 K and 1500 K. During the measurements the base pressure in the photoemission chamber was in the $10^{-11}$ mbar range, allowing sampling times of about one hour without changing the adsorbate overlayer.

## 2. Spinresolved spectra of Ar monolayers

Spinresolved photoemission from argon atoms in the adsorbate phase is of interest because for such light atoms ($Z = 18$), spin–orbit interaction, which is responsible for a photoelectron polarization, is weak. The fine-structure splitting of the final ionic states $Ar^+ 3p^5(^2P_{3/2}, {}^2P_{1/2})$ in the gas phase is 180 meV only, whereas those of Kr ($Z = 36$) and Xe ($Z = 72$) are 0.6 and 1.3 eV, respectively. Nonetheless, the photoelectron spin polarization in valence-shell photoemission from *free* Ar atoms has almost the same quantitative values as for free Kr and Xe atoms – provided the fine-structure splitting is experimentally resolved [8]. The gas-phase results show that the strength of spin–orbit interaction primarily determines the quantitative splitting of energy levels but not the degree of the photo ESP.

For atoms on a surface we would expect in principle the same behavior but, on the other hand, there are two mechanisms which change the situation. First, all photoemission lines are broadened due to lifetime and vibrational effects so that a small level splitting could possibly be washed out. Second, in addition to spin–orbit coupling the anisotropic bonding interaction comes into play which is induced by the presence of the substrate surface and by the neighboring adatoms. The latter leads to the well-known magnetic $|m_j|$-sublevel splitting in adsorbed Xe and Kr layers [3, 9, 10].

Figure 1 shows a spin-resolved photoelectron spectrum of Ar on Pt(111) at monolayer coverage. The spectrum has been taken with circularly polarized synchrotron radiation of $h\nu = 14$ eV at normal incidence and normal emission. The total intensity (upper panel) is essentially given by one peak around 7.7 eV binding energy with respect to the Fermi energy of the platinum substrate. The photon bandwidth $\Delta h\nu$ and

* This paper was contributed to the 8th Vacuum Ultraviolet Radiation Physics International Conference, held in Lund, Sweden, 4–8 August, 1986, and will be included in part II of the Conference proceedings. (Editors: P. -O. Nilsson and J. Nordgren).

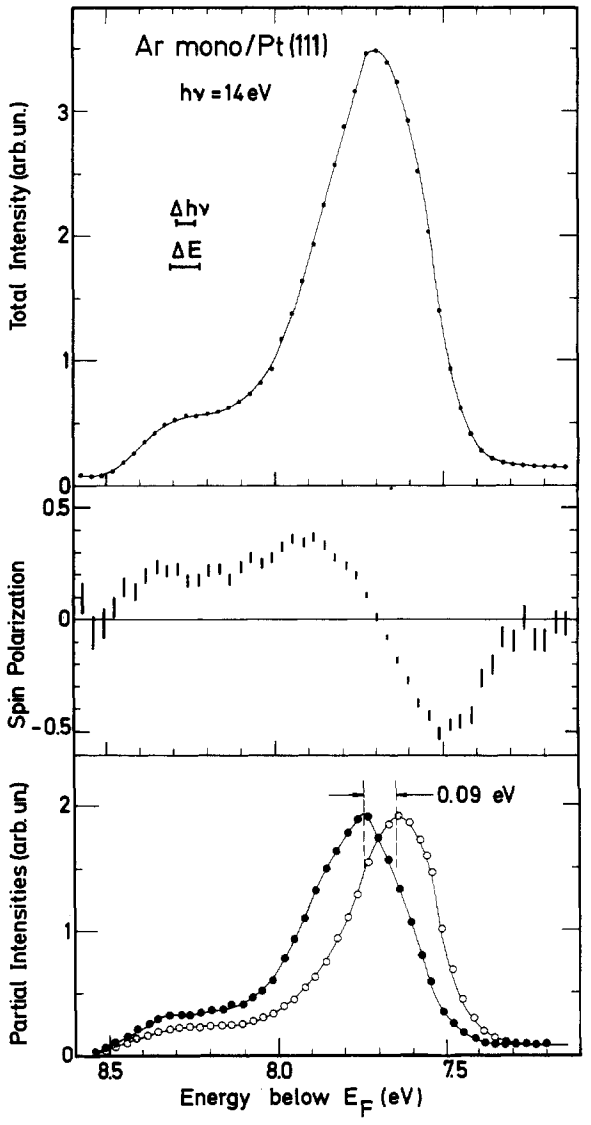


*Fig. 1.* Spin-resolved photoelectron spectrum of an Ar monolayer on Pt(111) at normal incidence and emission. Upper panel: total photoelectron intensity; middle panel: photo ESP; lower panel: partial spin-up (●) and spin-down (○) intensity curves derived from the total intensity and spin polarization.

the energy resolution of the photoelectron spectrometer $\Delta E$ (FWHM) are given by bars, which show that the energetic resolution is considerably smaller than the width of the photoemission peak. The corresponding spin-polarization spectrum (middle panel) shows that there is a spin-down/spin-up substructure hidden under the intensity peak of the upper panel. The ESP values have been normalized to complete circular photon polarization; error bars represent one standard deviation and include systematic errors of the ESP analysis. The sign convention is such that $P = +1$ $(-1)$ if the electron and photon spins are parallel (antiparallel).

The substructure in the intensity feature can most clearly be seen when we derive the partial spin-up and spin-down intensities $N_\uparrow$, $N_\downarrow$ from the total intensity and the ESP according to

$$N_\uparrow = \frac{N}{2}(1 + P) \qquad N_\downarrow = \frac{N}{2}(1 - P). \tag{1}$$

Here $N = N_\uparrow + N_\downarrow$ represents the total intensity. Equation (1) follows directly from the basic definition of the ESP

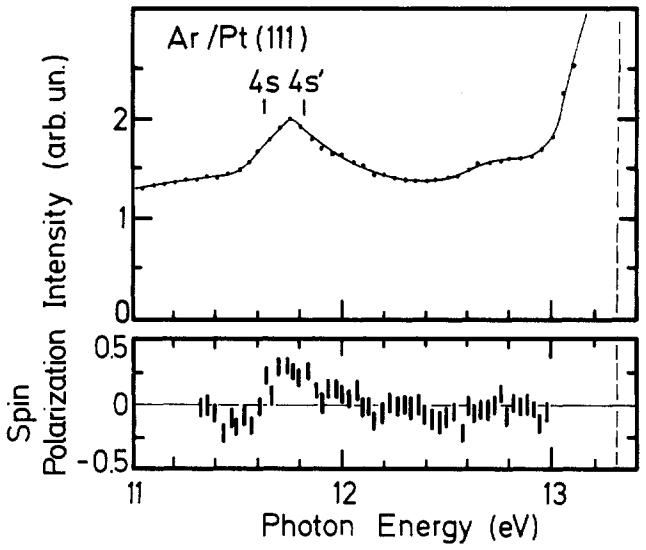


*Fig. 2.* Spectral variation of electron intensity and ESP for an Ar monolayer on Pt(111) in the region of the atomic $3p \rightarrow 4s$, $4s'$ resonance lines (bars). The vertical dashed line denotes the threshold for direct photoemission from the Ar $3p$ valence orbital.

$$P = \frac{N_\uparrow - N_\downarrow}{N_\uparrow + N_\downarrow}. \tag{2}$$

The partial intensities obtained using eq. (1) are plotted in the lower panel of Fig. 1. These spectra clearly reveal two peaks of opposite spin orientation being separated by a spacing of only 90 meV. Since the widths of the two photoemission peaks are about 300 meV FWHM, the substructure is almost unobservable in the total photoemission intensity. The two partial peaks reflect the spin-up and spin-down parts of the $p_{xy}$-orbital of the adsorbed Ar atoms, as has been recently discussed in detail [6] by comparison with the heavier noble gases.

For the same adsorbate we have observed photon-induced resonances due to excitation of a $3p$ valence electron into the empty $4s$ orbital. The result of this measurement is shown in Fig. 2, which gives the electron intensity and ESP at a fixed electron kinetic energy just above the low-energy cut-off (see below) as function of photon energy. A resonance feature of about 200 meV FWHM appears at the position of the $3p \rightarrow 4s$ resonance doublet of *free* argon atoms (marked positions, from Ref. [11]). There are no resonances at photon energies less than 11 eV. Thus we find that in Ar adatoms on the Pt(111) surface the first optical dipole transition ($3p \rightarrow 4s$) appears almost unshifted if compared with the gas phase. A similar behavior was found for the heavier noble gases [4, 6]. Whereas the intensity feature does not show significant structure, the ESP curve reveals that there is both a spin-down and a spin-up contribution contained in the resonance. However, the structure is too weak to allow for a detailed decomposition. Note that direct photoemission from the Ar $3p$ valence orbital sets in only at 13.3 eV (dashed line in Fig. 2). After Ar desorption all features vanish.

### 3. Xe monolayers on Ir(111) and graphite(0001)

The new "sub-threshold" resonance mechanism is further illustrated by the series of spectra for Xe on Ir(111) displayed in Fig. 3. The spectra have been taken at photon energies in the region of the strong atomic Xe $5p \rightarrow 6s$ resonance lines.

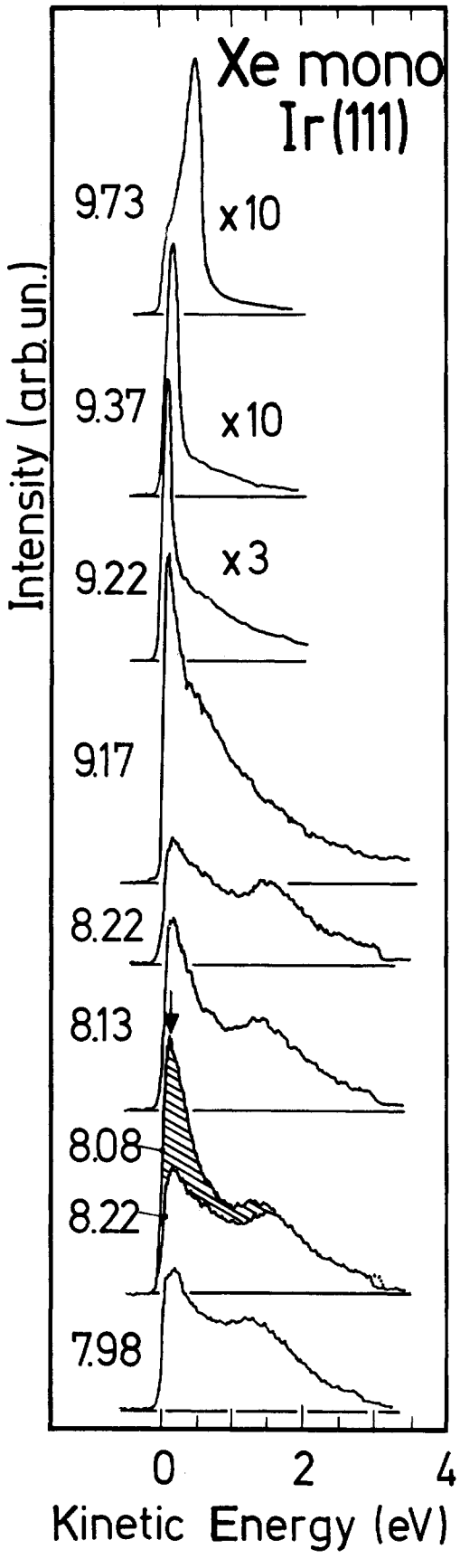


*Fig. 3.* Electron spectra of a Xe Monolayer on Ir(111) taken for various photon energies at normal incidence and emission.

They reveal a sudden enhancement of the electron intensity at small kinetic energies (hatched area) when going from $h\nu$ = 7.98 eV to 8.08 eV, which vanishes again upon a further increase of photon energy to 8.22 eV (error of absolute photon energy: 60 meV). Only at 9.17 eV the first photoemission peak begins to emerge from the low-energy cut-off of the spectrum and its intense maximum is fully developed at 9.37 eV, then it starts to shift to higher kinetic energies as visible in the 9.73 eV spectrum. Thus, the resonant enhancement (hatched area) occurs more than 1 eV below the threshold for direct photoemission. A similar behavior has been observed on the Pt(111) and graphite(0001) substrates [4, 6].

The full spectral variation of electron intensity and ESP is illustrated in Fig. 4 for a monolayer of Xe on the basal plane of natural single-crystal graphite. The figure exhibits the sharp 6*s*-resonances with their corresponding characteristic ESP curve [4] *below* the first threshold for direct photoemission (vertical dashed line) and the broader resonance features occurring in the photoemission channels *above* thresholds. The curve below threshold has been obtained by setting the spectrometer at a fixed electron energy just above the low-energy cut-off of the spectrum (arrow in Fig. 3) while scanning the monochromator (constant-kinetic-energy spectroscopy). In contrast, for the curves above threshold a programmable power supply kept the spectrometer always at the maximum of the photoemission peak during the monochromator scan (constant-final-ionic-state spectroscopy). In all three channels, corresponding to different final ionic states, the photoemission intensities just above thresholds are strongly enhanced. The hatched peaks in intensity and ESP in channel 2 are most likely due to excitation of the Xe 7*s* level as is evident from a comparison of corresponding curves of several different Xe overlayers [6]. The features in channel 1, especially the deep minimum in intensity (and ESP) at $h\nu$ = 12 eV are not yet understood.

## 4. Coverage dependence of spectra and resonances for Xe on Ir(111)

A point of high interest is the coverage dependence of the resonances. We have studied this issue for the system Xe on Ir(111) at coverages from the sub-monolayer regime up to the three-dimensional Xe crystal. These measurements have shown that substantial changes of the resonance features and of the photoemission spectra occur when the coverage is increased.

The overlayers were characterized in the following way: In the commensurate $\sqrt{3} \times \sqrt{3}$ (R 30°) overlayer all adatoms occupy identical adsorption sites (threefold hollow sites) corresponding to a Xe–Xe distance of 4.7 Å. This adsorbate phase is characterized by the well-known sharp LEED pattern. Upon dosing more Xe to the commensurate $\sqrt{3}$ overlayer a rather complicated compression phase occurs in which rotated domains are formed [12]. At monolayer saturation coverage an incommensurate hexagonal close-packed layer is formed. The weakly temperature-dependent Xe–Xe distance is 4.40 ± 0.05 Å at a substrate temperature of 58 ± 4 K. Such close-packed monolayers were adsorbed by saturating the coverage at a temperature slightly above the sublimation point of the second layer. Formation of the commensurate $\sqrt{3}$ layer as well as monolayer completion was monitored by the characteristic photoelectron spectra shown in Fig. 5. These high-resolution spectra were taken at normal incidence and normal emission and at an angular resolution of $\Delta\theta = \pm 3°$. The series of spectra reveals that, like on the Pt(111) substrate [3], the 6% difference of the

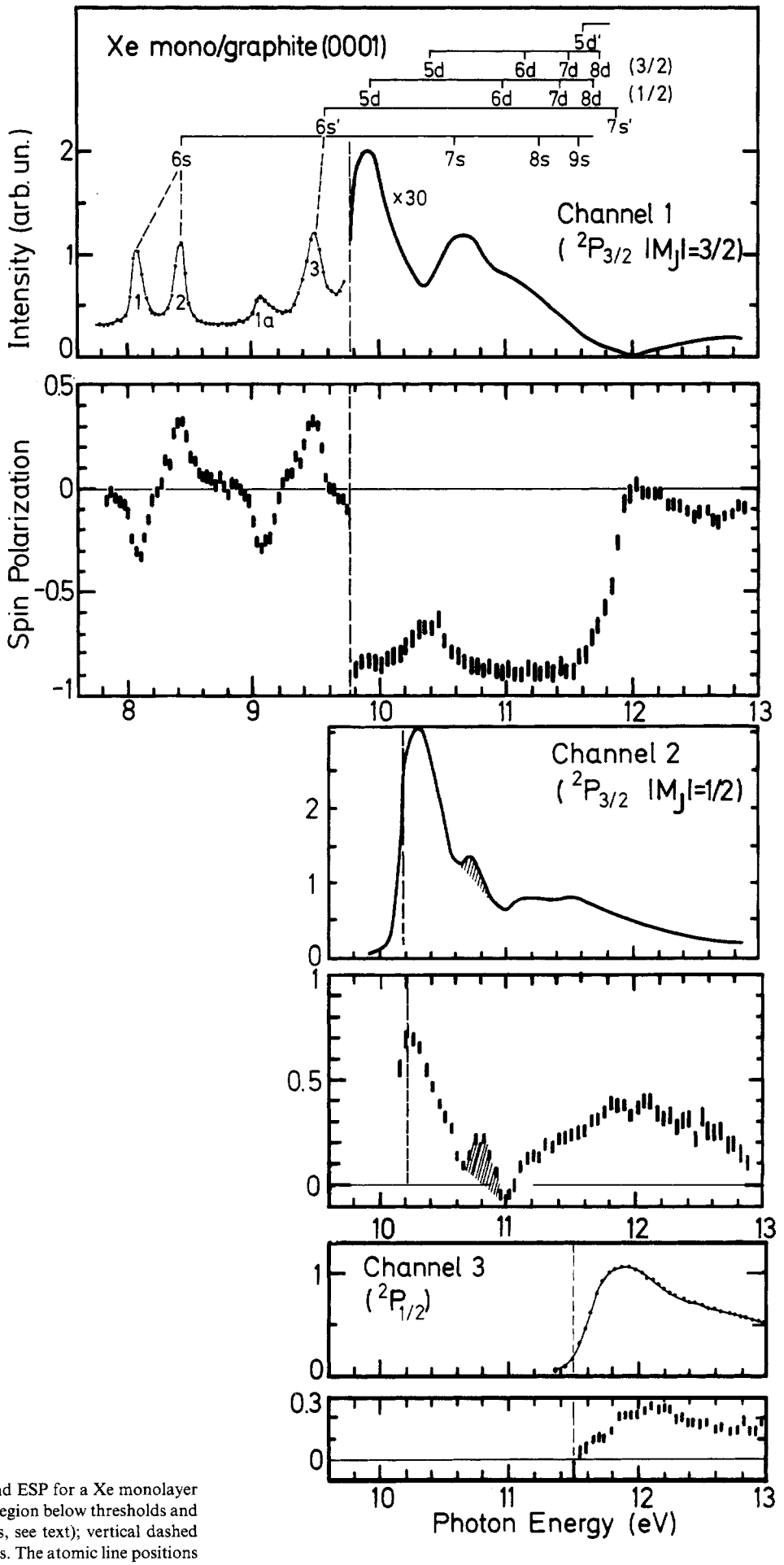


*Fig. 4.* Spectral variation of electron intensity and ESP for a Xe monolayer on graphite. Data are given for the 6*s*-resonance region below thresholds and for the three photoemission channels (for details, see text); vertical dashed lines denote the corresponding threshold positions. The atomic line positions on top of the figure are from Ref. [11].

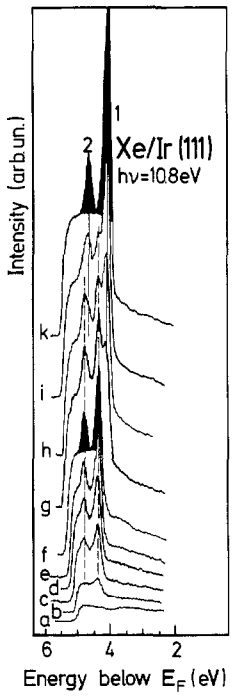


*Fig. 5.* Highly-resolved photoelectron spectra of Xe on Ir(111) at various coverages. The series shows only the $|m_j| = 3/2$ and 1/2 components of the $p_{3/2}$ hole state (peaks 1 and 2, respectively). (a) Clean substrate; (b–f) Growth of commensurate $\sqrt{3} \times \sqrt{3}$ (R 30°) islands (Xe–Xe distance 4.70 Å); (g–i) Coexistence of $\sqrt{3}$ and incommensurate close-packed configurations; (k) Saturated close-packed monolayer (Xe–Xe distance 4.40 ± 0.05 Å).

lateral Xe–Xe distance between the commensurate $\sqrt{3}$ and the close-packed configuration leads to a marked change of the spectra (curves f and k, respectively). Upon overlayer compression, peaks 1 and 2 (hatched), corresponding to the $p_{3/2}|m_j| = 3/2$ and $p_{3/2}|m_j| = 1/2$ ionic hole states, are *shifted to lower binding energies* by 510 and 370 meV, respectively. Correspondingly, the $|m_j|$-sublevel splitting of the $p_{3/2}$ hole state increases by 140 meV, from 430 to 570 meV (all energy values have an uncertainty of 30 meV).

The coverage dependence of the 6*s* resonances in the spectral region *below* the direct-photoemission threshold is summarized in Fig. 6. Notice the different physical nature of the features displayed in Figs. 5 and 6. In Fig. 5 the abscissa is the binding energy or, apart from an additive constant, the photoelectron kinetic energy. Thus the photoemission peaks in Fig. 5 reflect the energy (and energy differences) of the *final ionic states reached from the ground state* via a direct bound free transition at a fixed photon energy. In contrast, Fig. 6 gives constant kinetic energy spectra and the abscissa is the photon energy, i.e., the peaks occur at energies matching a *discrete transition between the adsorbate ground and excited state.*

The resonance spectrum for the $\sqrt{3}$ overlayer (curve a) shows four distinct resonances which, by a comparison with Fig. 4, can be identified as the split Xe 6*s*-line (peaks 1 and 2) and the non-split Xe 6*s*′-line (peak 3). The fourth peak, denoted as 1a, very likely represents the $n = 2$ excitonic transition derived from the 6*s*-line, which occurred in all Xe overlayers studied so far (cf. Fig. 4 and Refs. [4] and [6]). Its existence indicates that the valence-orbital overlap of neighboring adatoms gives rise to excitons in the 2D adsorbate system, which bear much resemblance to the surface excitons in rare-gas solids investigated by Saile *et al.* [13].

The shift of energy levels observed in the photoemission

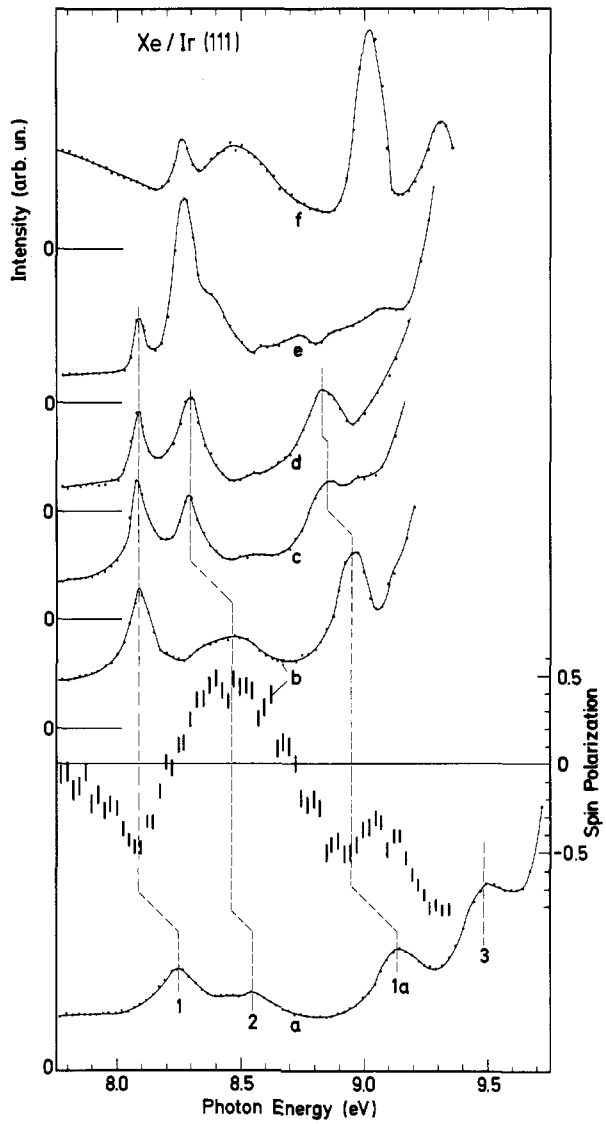


*Fig. 6.* Coverage dependence of electronic resonances for Xe on Ir(111). (a) Commensurate $\sqrt{3} \times \sqrt{3}$ (R 30°) overlayer; (b) Incommensurate hexagonal close-packed monolayer; (c) 2 (± 0.2) layers; (d) 3 (± 0.5) layers; (e) 5 (± 1) layers; (f) Annealed Xe(111) crystal, 15–20 layers.

spectra (Fig. 5) also shows up in the positions of the 6*s*-resonances (Fig. 6). When going from the $\sqrt{3}$ layer (curve a) to the incommensurate monolayer (curve b) the resonances are red shifted (i.e., towards lower photon energies). In addition, the threshold for direct photoemission is lowered to $h\nu = 9.27$ eV, so that resonance 3 can no longer be observed below threshold. The shift of resonances 1 and 2, corresponding to the $p_{3/2}|m_j| = 3/2$ and $p_{3/2}|m_j| = 1/2$ core-hole configurations, is 160 and 100 meV, respectively. Correspondingly, the $|m_j|$-sublevel splitting of the $p_{3/2}$ core-hole configuration increases by 60 meV (from 310 to 370 meV). Thus the increasing valence-orbital overlap during the commensurate → incommensurate phase transition causes a rise in the Xe 5*p* level positions, which is reflected in a decrease of both the 5*p* binding energy and the $5p \rightarrow 6s$ excitation energy. The decrease of the $5p \rightarrow 6s$ excitation energy is smaller than the decrease of the 5*p* binding energy probably because the 6*s*-level is also shifted during overlayer compression.

For coverages exceeding one monolayer (curves c–f), the resonance features again change significantly. Formation of the second layer (curve c) leads to a marked red shift (180 meV)

of resonance 2. This can be qualitatively explained by taking the spatial orientation of the core-hole states [6] into consideration: Resonance 2 is associated with a $p_{xy}$–$p_z$ (hybrid) core state and is therefore more affected by neighboring adatoms in the second layer (i.e., in $z$-direction) than resonance 1, having a pure $p_{xy}$ core hole which extends essentially parallel to the surface. The position of resonance 1 is almost unaffected by the second Xe layer.

With increasing coverage, the relative intensity of the 8.1 eV-peak decreases as visible in the spectra for three and five layers (curves d and e, respectively), until for the Xe(111) crystal (curve f) it is completely absent. We conclude that this peak occurs for atoms in the first layer only, where due to the contact with the surface the symmetry is reduced as compared to the symmetry of a Xe atom in the bulk of the rare-gas crystal. A comparison of the corresponding valence band structures for a Xe monolayer and the Xe crystal further supports this explanation [6]. Comparison of curve f with the absorption spectrum of solid Xe measured by Saile (Fig. 3.10 in Ref. [14]) suggests that the narrow peak around 8.3 eV is the surface exciton ($n = 1$) occurring in the topmost layer, whereas the broad feature around 8.5 eV is the volume exciton ($n = 1$).

## 5. Conclusions

New energy-, angle-, and spin-resolved photoemission data for Ar and Xe adsorbed on the (111) faces of platinum and iridium and on the basal plane of natural single-crystal graphite have been presented. The photoelectron spin orientation is induced via optical pumping with circularly polarized synchrotron radiation from the storage ring BESSY. Our results have shown that in the adsorbate – like in the gas phase – considerable ESP values of over 50% occur even for a light atom such as argon. This demonstrates that the new method is principally not restricted to high-$Z$ systems. Moreover, the partial spin-up and spin-down spectra determined from the total photoelectron intensity and the ESP spectrum, resolved a doublet with a spacing of only 90 meV, which is hardly discernible in the total intensity. In addition to these data for direct photoemission from the Ar $3p$ valence orbital we have found evidence for discrete Ar $3p \rightarrow 4s$ excitations at photon energies very close to the corresponding line positions for free atoms.

For xenon monolayers on graphite and iridium(111) evidence of discrete Xe $5p \rightarrow 6s$, $6s'$ excitations below the threshold for direct photoemission have been presented. The $6s$-line is split due to the anisotropic interactions in the adlayer, but the excitation energies are close to the atomic line positions. Above the photoemission threshold an autoionization-like feature occurs which is very likely caused by interference of a discrete excited configuration (probably $7s$) with the open photoemission continuum.

For the system xenon on iridium(111) we have investigated the coverage dependence of the Xe $5p \rightarrow 6s$ resonances when going from the sub-monolayer regime via the close-packed monolayer and multilayers up to the 3D rare-gas crystal. Substantial changes in the resonance positions and intensities occur which are attributed to the increasing valence-orbital overlap upon overlayer compression and to the change of point symmetry when going from the monolayer to the 3D crystal.

## Acknowledgements

We would like to thank A. Eyers, U. Friess and F. Schäfers and the BESSY staff for useful cooperation. The Ir crystal was kindly provided by T. Rhodin (Cornell University, Ithaca) and B. Addiss (Materials Preparation Laboratory of Cornell University) and the graphite crystal was kindly provided by T. S. Noggle (Oak Ridge Nat. Lab.). This work was financially supported by BMFT (05331AX).

## References

1. Heinzmann, U. and Schönhense, G., in Polarized Electrons at Surfaces (Edited by R. Feder), Ch. XI, p. 467 ff., World Scientific, Singapore (1985); Heinzmann, U., Proceedings of VUV 8 (inv. talks), Physica Scripta in press 1987, Vol. 35.
2. Eyers, A., Schäfers, F., Schönhense, G., Heinzmann, U., Oepen, H. P., Hünlich, K., Kirschner, J., and Borstel, G., Phys. Rev. Lett. **52**, 1559 (1984).
3. Schönhense, G., Eyers, A., Friess, U., Schäfers, F., and Heinzmann, U., Phys. Rev. Lett. **54**, 547 (1985).
4. Schönhense, G., Eyers, A., and Heinzmann, U., Phys. Rev. Lett. **56**, 512 (1986).
5. Natural single crystal graphite from Lead Hill Mine, Ticonderoga, New York.
6. Schönhense, G., Appl. Phys. **A41**, 39 (1986).
7. Schäfers, F., Peatman, W., Eyers, A., Heckenkamp, Ch., Schönhense, G., and Heinzmann, U., Rev. Sci. Instrum. **57**, 1032 (1986).
8. Heinzmann, U., Schönhense, G., and Kessler, J., Phys. Rev. Lett. **42**, 1603 (1979); J. Phys. **B13**, L153 (1980).
9. Waclawski, B. J. and Herbst, J. F., Phys. Rev. Lett. **35**, 1594 (1975).
10. Horn, K., Scheffler, M., and Bradshaw, A. M., Phys. Rev. Lett. **41**, 822 (1978); Scheffler, M., Horn, K., Bradshaw, A. M., and Kambe, K., Surf. Sci. **80**, 69 (1979).
11. Moore, C. E., Atom. En. Lev. Vol. III, NBS, U.S.A. (1958).
12. Kern, K., David, R., Palmer, R. L., and Comsa, G., ECOSS-8, Jülich (1986), book of abstracts, p. 174; Phys. Rev. Lett. **56**, 620 (1986).
13. Saile, V., Skibowski, M., Steinmann, W., Gürtler, P., Koch, E. E., and Kozevnikov, A., Phys. Rev. Lett. **37**, 305 (1976).
14. Schwentner, N., Koch, E. E., and Jortner, J., Electronic Excitations in Condensed Rare Gases, Springer Tracts in Modern Physics, Vol. 107 (1985).